Open ocean biogeochemical impacts of extreme terrestrial precipitation

Shailja Gangrade[1], Mara A. Freilich[1,2], Élise Beaudin[1,3], Kelly Luis[4], Inés M. Leyba[5], Melissa M. Omand[6], Sarah E. Lang[6], Jeff S. Bowman[7], Larry O'Neill[5], and Dante A. Capone[7]

[1]Brown University, Department of Earth, Environmental, and Planetary Sciences
[2]Brown University, Division of Applied Mathematics
[3]Ocean Networks Canada, University of Victoria, Victoria, British Columbia, Canada
[4]Jet Propulsion Laboratory, California Institute of Technology
[5]Oregon State University
[6]University of Rhode Island, Graduate School of Oceanography
[7]University of California San Diego, Scripps Institution of Oceanography

Key Points:

- Anomalously high precipitation from atmospheric rivers led to elevated river discharge, low ocean salinity, and increased stratification
- Freshwater discharge was rapidly transported hundreds of kilometers offshore, to the open ocean, within submesoscale eddies and filaments
- The biogeochemical impacts of runoff vary depending on nutrient properties at the coastal source and mixing along water-parcel trajectories

Corresponding author: Shailja Gangrade, shailja_gangrade@brown.edu

Abstract

Extreme events reshape ocean ecosystems with significant implications for nutrient and carbon cycling. Here, we demonstrate that flooding on land can be a significant driver of biogeochemical variability in the open ocean, even in relatively dry climates. Using satellite observations, in situ measurements, and Lagrangian particle tracking, we present evidence that freshwater discharge from extreme precipitation during the 2023 water year was transported into the oligotrophic region of the California Current System. This transport was facilitated by submesoscale eddies and filaments and resulted in significant anomalies in surface salinity, stratification, nutrient concentrations, as well as phytoplankton and bacterioplankton community composition. These observations, combined with an Earth system model, highlight the importance of episodic river discharge events in shaping offshore biogeochemical fluxes and ecosystem structure in eastern boundary current systems under a changing climate.

Plain Language Summary

In 2023 along the US West Coast, record breaking precipitation, due to weather features called atmospheric rivers, led to flooding on land and increased river runoff into the ocean. Using model estimates alongside ship and satellite observations, we demonstrate that the increase in freshwater discharge into seawater environments had a striking effect on the physics and biology of both the coastal and open ocean. In particular, this extreme terrestrial precipitation was associated with reduced ocean salinity, as well as growth and accumulation of phytoplankton. River estuaries, such as the San Francisco Bay, are typically enriched in nutrients, such as nitrate and phosphate. Therefore, we detected that as river runoff waters were rapidly transported hundreds of kilometers offshore through circulating current features, they also carried unique microbial communities potentially influenced by these terrestrial nutrient sources. However, runoff waters rich in phytoplankton did not always have the same composition of nutrients, nor were they made up of the same biological communities. Therefore, future studies are needed to further document and evaluate how extreme precipitation affects ocean ecosystems and circulation.

1 Introduction

Extreme precipitation over the US west coast is projected to increase in frequency (Swain et al., 2018), which will have cascading effects on society and ecosystems. A likely direct impact will be an increase in flooding, resulting in increased episodic river discharge into the ocean. Parts of the western US coastal region host a relatively dry climate that does not typically experience large river discharges. Analysis of a climate model ensemble, the Community Earth System Model Large Ensemble (CESM2 LENS), suggests that extreme river discharge into the ocean along the US West coast is likely to increase through the end of the century under a moderate climate change scenario (Figure 1A) alongside increased precipitation (Swain et al., 2018). River runoff has been observed to lead to enhanced coastal primary production (Kessouri et al., 2021) and modify global carbon cycling (Regnier et al., 2022). However, connections between extreme wet events, changes in ocean surface salinity (Hoffman et al., 2022), and the ultimate effects on biogeochemical fluxes remain poorly understood. Therefore, here we document the physical and biogeochemical impacts of extreme precipitation and flooding on the open ocean in a mid-latitude eastern boundary current system using observations during a recent high precipitation season.

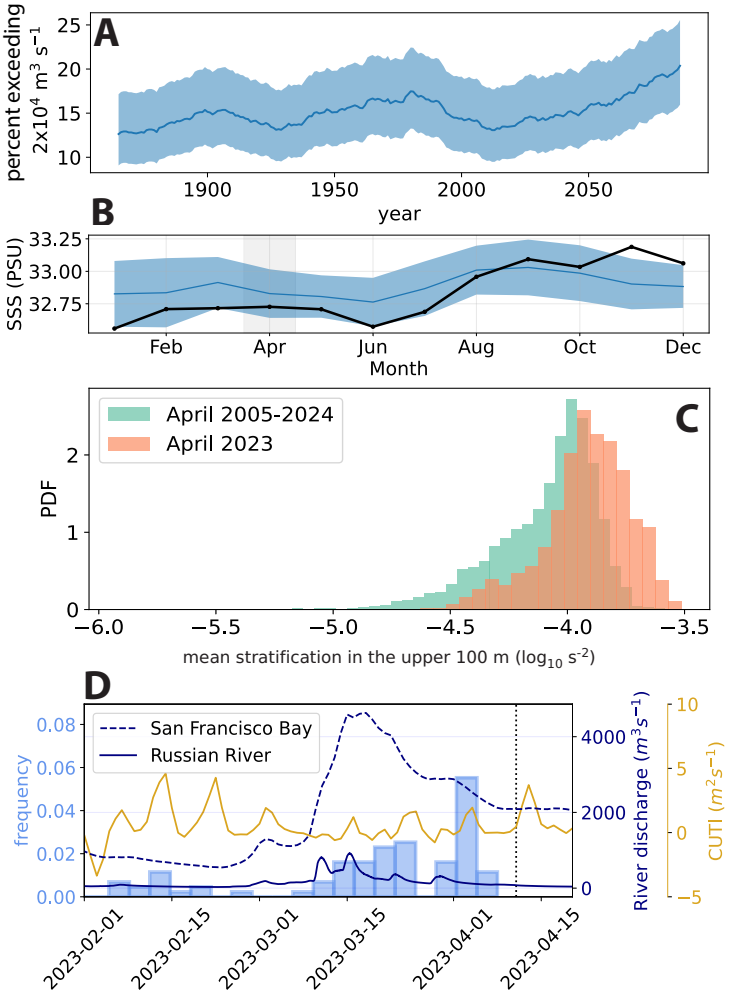

Figure 1. (A) Extreme river discharge to the ocean from the climate model ensemble CESM-LENS2 quantified as percent of 90 ensemble members with April discharge exceeding $2 \times 10^4\ m^3\ s^{-1}$ integrated over the entire US West Coast. Shading is the 75% confidence interval. (B) Monthly average salinity and standard deviation (blue; 2015–2025, except 2023) in the California Current System offshore of San Francisco from the SMAP satellite. Black line is monthly average in 2023. (C) Probability density functions of mean stratification (calculated as the Brunt-Väisälä frequency N^2) in the upper 100 meters from the California Underwater Glider Network Line 66.7. Distributions are significantly different (Kolmogorov-Smirnov test: $D = 0.346$, $p < 0.01$) (D) Histogram in light blue showing date at which high-Chl (Chl-a $> 1\ mg\ m^{-3}$) waters, tracked backward in time using GLORYS horizontal current velocities, reach the coast. River discharge is in dark blue and the Coastal Upwelling Transport Index (CUTI) is in yellow.

2 Materials and Methods

Observations were collected during the NASA Sub-Mesoscale Ocean Dynamics Experiment (S-MODE) Intensive Operations Period "IOP2" (Farrar et al., 2025). Sampling occurred from April 3–May 2, 2023 within an operations area 100–300 km off of San Francisco, California.

Precipitation estimates and integrated vapor transport (IVT) were obtained from the high-resolution ERA5-Land and ERA5 reanalysis, respectively. Daily discharge measurements of the Russian River (Hacienda Bridge monitoring location) were obtained from USGS, and daily outflow estimates for the San Francisco Bay were obtained from California Natural Resources Agency Dayflow product.

Future river discharge is modeled using CESM2 Large Ensemble, which uses Model for Scale Adaptive River Transport MOSART1.0. We used the historical and SSP3-7.0 scenarios integrated over the US West coast and analyzed the proportion of the ensemble members with discharge exceeding $2\times10^4\ m^3\ s^{-1}$, which is 96th percentile of discharge. A 30-year running mean was calculated prior to plotting, following the methods of Swain et al. (2018).

Physical and hydrographic patterns of the coastal and open ocean were investigated using salinity, stratification, and upwelling measurements. Monthly sea surface salinity (SSS) was retrieved from the Soil Moisture Active Passive (SMAP) mission Level-3 v6.0 data with a spatial resolution of approximately 0.25 degrees. The SSS product was averaged for the S-MODE operations area (Farrar et al., 2025). Mean stratification in the upper 100 meters were calculated as the Brunt-Väisälä frequency (N^2) from depth-dependent density profiles obtained from California Underwater Glider Network data from 2015–2025 on Line 66.7, located off Monterey Bay, California. Fluctuations in wind-driven upwelling fluxes were characterized using the Coastal Upwelling Transport Index (Jacox et al., 2018).

Water parcel tracking simulations were conducted by seeding particles in high Chl regions (surface concentration $> 1\ mg\ m^{-3}$) identified from a satellite-derived sea-surface Chl-a image from April 11, 2023 (during S-MODE IOP2). These particles were tracked backward in time (with a time step of 1 day) using GLORYS horizontal velocities (0.083-degree spatial resolution). A date to coast was computed for each water parcel as the duration it took for each particle to reach the coastline, backward in time, from its initialized location.

Macronutrients, phytoplankton pigments, and particulate organic carbon (POC) concentrations were analyzed in samples collected from the shipboard underway system during S-MODE IOP2 (Farrar et al., 2025). Nutrients (e.g., NO_3, PO_4) were analyzed colorimetrically with a Quickchem 8500 Lachat Flow Injection Analysis System, chlorophyll (Chl) and accessory pigments were analyzed with an Agilent RR1200 HPLC, and POC molarity was obtained using a Costech 4010 Elemental Analyzer. Underway POC measurements were also derived from an empirical fit between the beam attenuation coefficient at 657 nm, measured by a Seabird Scientific ac-s Spectral Absorption and Attenuation Sensor, and bottle POC concentrations (Lang et al., 2023). Underway Chl-*a* concentrations were derived from absorption line height at 676 nm measured by the ac-s sensor and were calibrated using extracted bottle samples analyzed by a Turner A10 fluorometer (Roesler & Barnard, 2013). Phytoplankton biomarker pigment concentrations were normalized by total Chl-*a* concentrations for subsequent analyses. Nitrate and phosphate surface bottle measurements were also obtained from the California Cooperative Oceanic Fisheries Investigation (CalCOFI) from the time period 1954–2024.

DNA samples for 16S and 18S rRNA gene sequencing were collected from the shipboard underway system (near-surface waters) to determine bacterioplankton and eukaryotic phytoplankton community composition, respectively. For DNA samples, 0.5 L of sea-

water was filtered through a sterile 0.2 µm Supor membrane disk filter, stored at -80°C, and extracted using a KingFisher Flex Purification System and MagMax Microbiome Ultra Nucleic Acid Extraction kit following the methods of Merz et al. (2026). The V4–V5 hypervariable region of the 16S rRNA gene and V9 region of the 18S rRNA gene were amplified and sequenced using the MiSeq platform (Illumina) with universal primers 515F and 806R for 16S rRNA gene sequencing, 1380F and 1505R for 18S rRNA gene sequencing, and a 2×151 bp library architecture. Amplicon sequence variant (ASV) reads were filtered, denoised, and merged with DADA2 (Callahan et al., 2016) and analyzed with paprica v0.7.1 (Bowman & Ducklow, 2015). Paprica uses RefSeq (O'Leary et al., 2016) and PR2 (Guillou et al., 2012) as reference databases and assigns taxonomy using a phylogenetic placement approach, where each ASV is placed onto a pre-computed phylogenetic tree with Infernal (Nawrocki & Eddy, 2013), epa-ng (Barbera et al., 2019), and Gappa (Czech et al., 2020). Reads assigned as metazoan mitochondria or chloroplasts were omitted. Libraries with sizes below the 5th percentile and reads with abundances fewer than 10 were eliminated. These thresholds were implemented to remove potential contaminant reads and did not significantly alter community composition analyses. Phytoplankton were identified using taxonomic labels for each sequence.

Principle Coordinate Analysis (PCoA) of Bray-Curtis distances and Redundancy Analysis (RDA), both using Hellinger-transformed relative abundances, were performed using the vegan package in R (Legendre & Gallagher, 2001; Oksanen et al., 2001). The RDA was conducted with 104 samples and using 8 environmental variables: temperature, salinity, density (sigma-T), dissolved oxygen concentration, photosynthetically active radiation (PAR), Chl-*a* concentration, Chl-*a* fluorescence, and particulate organic carbon concentration. Comparisons between nutrients (nitrate and phosphate) and sequencing-derived community composition were not possible due to limited overlap between sampling (only 9 samples).

High-Chl features, such as those associated with (sub)mesoscale eddies and filaments, were qualitatively identified and described in the S-MODE sampling region during April 2023 using sea-surface Chl-*a* products derived from MODIS Aqua and Sentinel-3 Ocean and Land Color Instrument (OLCI). From April 20–25, 2023, the ship identified and followed a cyclonic submesoscale eddy, and samples taken within this eddy were identified as "eddy-core" based on their Chl-*a* concentration (highest measured Chl-*a* near core) and relative vorticity values (relative maxima at core) derived from currents measured by DopplerScatt (Rodríguez et al., 2018; Wineteer et al., 2020) and a shipboard Acoustic Doppler Current Profiler (ADCP).

3 Results

3.1 Anomalous precipitation and freshwater discharge

The US West coast water year 2023 had anomalously high precipitation due to multiple landfalling atmospheric rivers (ARs) (DeFlorio et al., 2024; Jimenez Arellano et al., 2025). The number of storms, combined with the rapid succession of storms, led to record-breaking precipitation, exacerbated hydrological impacts, and high discharges into the coastal ocean.

In situ sampling that took place April 6–30, 2023 (near peak discharge and precipitation) during the S-MODE IOP2 (Farrar et al., 2025) in the offshore region of the California Current System (Figure 1) revealed that large discharge events impacted not only the coastal ocean, but also the more oligotrophic open ocean. A multiday AR event on March 10–15, 2023 with peak integrated vapor transport exceeding 750 $kg\ m^{-1}\ s^{-1}$ impacted the San Francisco (SF) Bay, Russian River, and Gualala-Salmon River watersheds immediately prior to sampling. From March 11–15, the event generated average daily integrated precipitation of 147.97 mm in the Russian and Gualala-Salmon water-

sheds and 101.37 mm in the SF Bay watershed. In the open ocean region off the coast of California, sea-surface salinity was anomalously fresh (low-salinity) during spring 2023, as observed in the SMAP salinity record (2015–2025; Figure 1B). The observed region was also significantly more stratified than in climatological conditions (Kolmogorov-Smirnov test: $p < 0.01$), in correspondence with the regionally low salinity that likely led to enhanced vertical density gradients (Figure 1C). Importantly, increased stratification can inhibit vertical mixing, in turn preventing the exchange of biogeochemical material between the surface and interior ocean, both near the coast and offshore.

3.2 Rapid across-shore transport of runoff waters

In contrast to a typical year where upwelling-driven productivity is associated with relatively high salinity (salinity > 33) (Gangrade et al., 2025; Zaba et al., 2021), some high-Chl features were associated with relatively low salinity (salinity ≤ 33), particularly in the offshore environment (Figure 2). Using Lagrangian methods to interrogate the water-parcel origins, we find that most of the high-Chl water parcels, observed up to 300 km offshore, originated near the Russian River estuary and near the SF Bay Estuary (Figure 1D, Supporting Information Figure 1). A forward tracking analysis of coastal water parcels using high-frequency radar fields also demonstrate that water parcels effectively escaped offshore to the open ocean (Supporting Information Figure 2).

The mode of the date of origin at the coast aligns with a runoff pulse that began on March 8, 2023, but some of the water parcels appear to have originated during an earlier upwelling pulse on February 15 (Figure 1D). The discharge during March 2023 from the Russian River and SF Bay (from estuaries with 70 m and 5 km widths, respectively) is of equivalent magnitude to the upwelling flux (CUTI) during this period. The observed open ocean water mass salinity is in the range 32.5–33.4. We anticipate that the freshwater discharge mixed with seawater both in coastal areas and offshore and therefore impacted the ocean environment hundreds of kilometers beyond the narrow coastal zone.

3.3 Distinct biogeochemical responses in the open ocean

We observed two distinct biogeochemical responses triggered by freshwater runoff into the open ocean. These responses, associated with waters of slightly different salinity ranges with potentially different origins, included differences in the composition of nutrients, phytoplankton, and bacterioplankton communities.

The majority of the water parcels that appear to have originated from within the SF Bay and Russian River estuaries were observed within a coherent submesoscale eddy (white box in Figure 2) which had the highest observed Chl concentration (approximately 6–8 $mg\ m^{-3}$) during sampling and an average particulate organic carbon concentration of 25 $mg\ m^{-3}$. Waters within the core of this eddy were of relatively low salinity (salinity ≈ 33) yet had anomalously high Chl. In the California Current System, waters of this salinity are typically much lower in Chl than our observations (Gangrade et al., 2025; Zaba et al., 2021). This feature also trapped water with very low nitrate:phosphate (N:P) ratios, indicating a probable estuarine source that may have alleviated micronutrient limitation, resulting in nitrate drawn down to near zero with excess phosphate (Figure 2B). The SF Bay Estuary, one of the likely major sources of these waters (Supporting Information Figure 1), is known to have excess phosphate (Cloern et al., 2020). The eddy feature also harbored a unique phytoplankton community with a predominance of fucoxanthin pigments, suggesting a diatom-dominated community. The eddy, with a radius of approximately 5 km, propagated westward at 6.5 $km\ d^{-1}$, generating an offshore carbon flux of 0.16 $mg\ m^{-2}\ d^{-1}$. This value is comparable to the average eddy flux of organic carbon in this system (Nagai et al., 2015). Submesoscale eddies such as this one are prevalent in the California Current System and are potentially a significant route of carbon supply to oligotrophic offshore regions through cross-shelf transport.

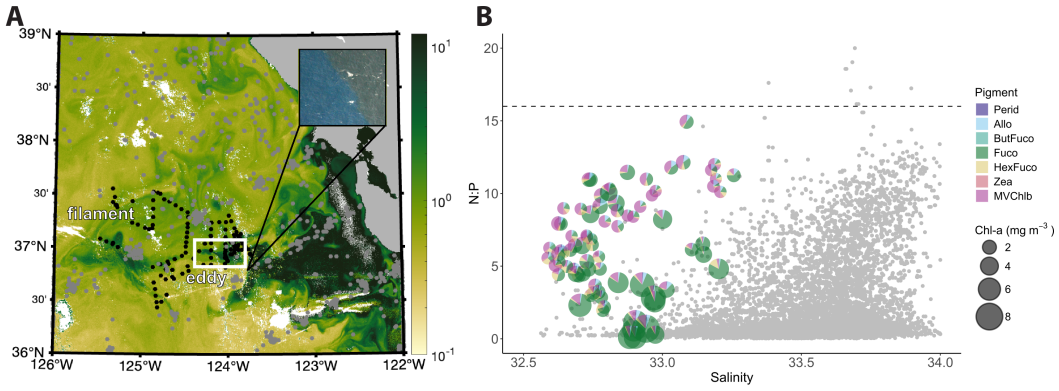

Figure 2. (A) Chl-a concentration in $mg\ m^{-3}$ observed by Sentinel-3A on April 22, 2023. Black dots show the locations of nutrient samples. Grey dots show locations of CalCOFI stations. The inset image is a photo taken from a twin otter airplane showing the boundary between high and low Chl waters. (B) Nitrate to phosphate ratio from surface CalCOFI observations, 1954–2024 (grey) and S-MODE observations (pie charts) as a function of salinity. The pie charts show the relative concentration of each pigment, normalized by the total Chl-a concentration ("Perid" for peridinin, "Allo" for alloxanthin, "ButFuco" for 19'-butanoyloxyfucoxanthin, "Fuco" for fucoxanthin, "HexFuco" for 19'-hexanoyloxyfucoxanthin, "Zea" for zeaxanthin, and "MVChlb" for monovinyl chlorophyll *b*). The pie size is proportional to Chl-a concentration. The horizontal dashed line is the Redfield ratio (16:1 N:P)

The remainder of the relatively low-salinity waters that were sampled were of lower salinity and Chl-*a* (salinity < 32.9 and mean Chl-*a* $= 1.7\ mg\ m^{-3}$) than the eddy waters. These waters, which appeared to be transported across-shore within a filament north of the eddy (Figure 2A), may have included: (1) water masses that advected north from the SF Bay Estuary along the coast; (2) water masses that originated from river runoff between Cape Mendocino and SF Bay, including the Russian River; or (3) waters of non-coastal, possibly sub-arctic, origin. Water-parcel tracking results indicate that the filament waters had some combination of these water source origins (Supporting Information Figure 1).

Despite these variable water mass origins, waters in this region were indeed anomalously fresh when compared with the historical CalCOFI record (1954–2024), consistent with the anomalously low regional salinity. Strikingly, these waters had relatively high N:P values when compared to waters of similar salinity in the historical record; however, these N:P values fell within the range of historical observations (5–12 µM N: µM P) for higher salinity waters. This may indicate mixing, along water mass trajectories, between coastally-originating freshwater with low N:P and seawater with relatively high N:P. Alternatively, N:P ratios in the source waters may be more similar to open ocean conditions. Waters of these salinity-nutrient conditions have occurred very infrequently in this region (Figure 2B).

Mixed phytoplankton communities were present in these anomalously low-salinity filament waters (Figure 2B). The increased proportion of the pigments that are monovinyl Chl-*b* and 19'-hex-fucoxanthin suggest a significant presence of chlorophytes (green algae) and prymnesiophytes, respectively. In these waters, the biogeochemical conditions indicate phytoplankton communities potentially limited by micronutrients: Chl was relatively low while macronutrients (nitrate and phosphate) were still available. This Chl

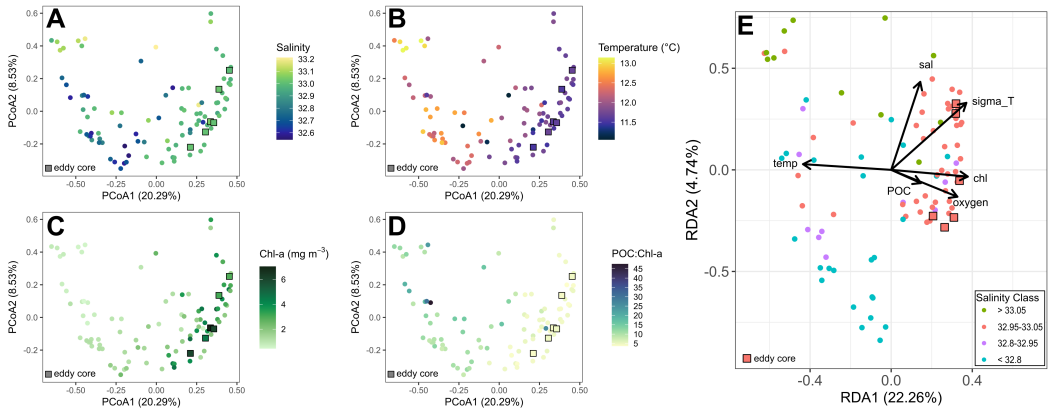

Figure 3. Principle Coordinate Analysis (PCoA) of eukaryotic phytoplankton community (from 18S rRNA gene sequencing) using Bray-Curtis dissimilarity, in which each point represents a sample and is colored by (A) salinity, (B) temperature, (C) Chl-*a* concentration, and (D) POC:Chl. Eddy core samples are identified with square markers. (E) Redundancy Analysis (RDA) of environmental variables, in which each point represents a sample, distinguished by salinity class (colors): salinity > 33.05, salinity between 32.95 and 33.05, salinity between 32.8 and 32.95, and salinity < 32.8. Eddy core samples are identified with square markers. Salinity, density (sigma-T), Chl-*a* concentration (chl), dissolved oxygen (oxygen), particulate organic carbon (POC), and temperature (temp) significantly drive eukaryotic phytoplankton community composition across sites ($p = 0.002$).

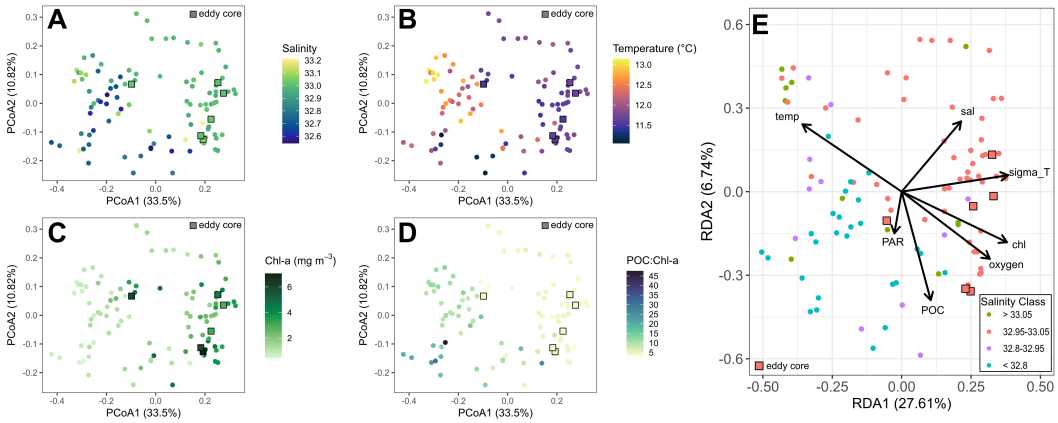

Figure 4. Principle Coordinate Analysis (PCoA) of bacterioplankton community (from 16S rRNA gene sequencing) using Bray-Curtis dissimilarity, in which each point represents a sample and is colored by (A) salinity, (B) temperature, (C) Chl-*a* concentration, and (D) POC:Chl. Eddy core samples are identified with square markers. (E) Redundancy Analysis (RDA) of environmental variables, in which each point represents a sample, distinguished by salinity class (colors):salinity > 33.05, salinity between 32.95 and 33.05, salinity between 32.8 and 32.95, and salinity < 32.8. Eddy core samples are identified with square markers. Salinity (sal), density (sigma-T), Chl-*a* concentration (chl), dissolved oxygen (oxygen), particulate organic carbon (POC), photosynthetically active radiation (PAR), and temperature (temp) significantly drive bacterioplankton community composition across sites ($p \leq 0.026$).

signal could also be attributed to an early bloom stage in which phytoplankton were beginning to respond to a recent nutrient injection (Catlett et al., 2021).

Salinity was significantly correlated with both eukaryotic phytoplankton and bacterioplankton community composition and had an effect distinct from other environmental variables (Figure 3 and Figure 4). Temperature and POC:Chl were also aligned with differences in eukaryotic phytoplankton and bacterioplankton community composition. Temperature, which typically has a strong positive but nonlinear relationship with nitrate (Palacios et al., 2013), and C:Chl are known to vary with phytoplankton and bacterioplankton size and community structure in this region (Taylor et al., 2015). Here, in particular, the effects of temperature and Chl-*a* concentration were different from the effects of salinity in driving eukaryotic phytoplankton and bacterioplankton community composition, as evidenced by the roughly orthogonal angles between these environmental variable vectors and the salinity arrow in canonical-axis space (Figure 3E and Figure 4E).

The effects of nutrients (nitrate and phosphate) on eukaryotic phytoplankton and bacterioplankton community composition could not be tested within this framework due to limited sampling overlap. However, distinct nutrient conditions indeed existed across a narrow range of observed salinity values (Figure 2B). These observations suggest that different nutrient conditions resulted in distinct biological communities between low and high salinity waters, but also between the low-salinity filament and low-salinity eddy core.

In particular we found that eukaryotic phytoplankton and bacterioplankton communities, derived from DNA sequencing, in the anomalously low-salinity filament were distinct from eddy-core communities. Certain chlorophytes within the genera *Ostreococcus*, *Bathycoccus*, and *Micromonas* were present together and higher in relative abundances in low-salinity filament waters than in waters of other salinity (Supporting Information Figure S3). Interestingly, these filament waters also contained elevated relative abundances of *Pseudo-nitzschia*, a toxigenic diatom species that is particularly competitive at transitions between iron-limited and iron-rich waters (Marchetti et al., 2012). In eddy-core waters, diatoms such as *Thalassiosira* were much higher in relative abundance than in filament waters. These observations are notably consistent with our HPLC-pigment derived observations. For bacterioplankton communities, *Alphaproteobacteria* (specifically the orders *Pelagibacterales* and *Rhodobacterales*) dominated in relative abundance in most waters across the observed salinity range; however, in the eddy-core waters, *Flavobacteriales* within the phylum *Bacteroidetes* contributed to a higher proportion of relative abundance than in low-salinity filament waters (and waters of salinity higher than the eddy-core) (Supporting Information Figure S4). Some bacteria in the phylum *Bacteroidetes* are known to have associations with phytoplankton blooms, particularly during bloom senescence (Teeling et al., 2016, 2012).

4 Discussion and Conclusion

Nearly all of the precipitation leading to flooding in northern California is due to ARs, which transport moisture from the tropics to the mid latitudes (Ralph et al., 2006; Bartusek et al., 2021). Extreme precipitation from ARs is projected to increase in frequency (Gershunov et al., 2019; Higgins et al., 2025), which may lead to increasing land-ocean connections due to increased river discharge. Riverine runoff is one part of the salinity budget in the California Current System, with advection and local precipitation also contributing, but it has unique implications for both circulation and biogeochemistry (Hoffman et al., 2022).

Nutrient conditions on land are typically different than in the open ocean, both in concentration and nutrient ratios. Terrestrial and coastal environments are also an important source of micronutrients such as iron, which is often limiting in the California

Current System (Johnson et al., 1999; Hogle et al., 2018). A release from micronutrient limitation may explain the low N:P ratios and predominance of diatom-associated pigments and ASVs in the observations. This shift in composition, consistently detected across phytoplankton sampling methods, could have ecological and biogeochemical implications. For example, diatom cells may sink more rapidly than other phytoplankton, potentially enhancing carbon export (Durkin et al., 2016; Kramer et al., 2025). Ultimately, we provide a nuanced view of the relevance of land-ocean nutrient transport: nutrient conditions similar to historical observations were associated with anomalously high Chl in a submesoscale eddy, while anomalous nutrient conditions (relatively high N:P) were associated with fresh (low-salinity) waters that are rarely sampled in this region. These observations add to prior literature suggesting large offshore blooms in response to anomalous precipitation (Kudela & Chavez, 2004). But importantly, the biogeochemical implications of riverine-sourced runoff appear to be idiosyncratic and may vary depending on the geographic origin, the timescale since origin, as well as the biogeochemistry of the source. The identification and characterization of water-mass origins are therefore needed to further elucidate connections between source-water properties and open-ocean ecosystem dynamics after extreme precipitation events.

The biophysical implications of runoff-supplied nutrient input merit further study. In contrast to upwelling filaments, freshwater runoff is relatively light due to its low salinity. The dynamics of light filaments contrast with those of dense filaments (McWilliams et al., 2015). Rather than sinking, light filaments may be dissipated by shear dispersion, resulting in an alternative pathway of carbon export and altered spatial distribution of offshore carbon flux and enhanced submesoscale lateral dispersion (Seitz & Freilich, 2025). These shear-driven eddy dynamics may result in enhanced offshore transport rather than enhanced subduction (Gruber et al., 2011). In addition, these observations highlight the need for a more nuanced understanding of the association between elevated Chl and eddies. Here, we showed the coherent trapping and offshore transport of waters elevated in Chl via a submesoscale eddy. Eddies, such as the one observed in this study, can therefore transport water quickly enough offshore to outpace phytoplankton loss due to grazing. However, more work is needed to understand the impact of other physical processes, like eddy-induced upwelling, and their interactions with biological growth and decay. Our observations demonstrate and provide further evidence that coherent submesoscale eddies facilitate cross-shelf exchange (Jhugroo et al., 2024), highlighting the need for future work to constrain their cumulative contributions.

Our observations suggest that increasingly extreme precipitation on land may have ecological impacts in eastern boundary currents due to changing the nutrient regime, particularly alleviation of micronutrient limitation. These results may also be applicable in other regions with episodic riverine influence in the open ocean such as the Chilean coast, where precipitation is also dominated by atmospheric rivers and becoming more extreme (Lagos-Zúñiga et al., 2024). Land management, such as methods targeting flood mitigation and nutrient runoff, has biogeochemical implications for the open ocean, even in relatively dry eastern boundary current regions.

Open Research Section

All S-MODE observational data are available on the NASA JPL PO.DAAC website: `https://podaac.jpl.nasa.gov/S-MODE`. S-MODE 16S and 18S rRNA gene sequencing data are available in the NCBI SRA Project TBD (submission in progress). River discharge measurements are available at `https://waterdata.usgs.gov/monitoring-location/USGS-11467000/`. San Francisco Bay outflow discharge data are available at `https://data.cnra.ca.gov/dataset/06ee2016-b138-47d7-9e85-f46fae674536/resource/f7c1ba7f-bd64-4762-88e3-6db9b2501b38/download/dayflowcalculations2023.csv`. Data from ERA5-Land are available at `https://doi.org/10.24381/cds.e2161bac`, and for ERA5 data at `https://doi.org/10.24381/cds.adbb2d47`. CalCOFI data are available at `https://`

calcofi.org/data/oceanographic-data/bottle-database/. CUGN data are available at https://spraydata.ucsd.edu/data-access. GLORYS and AVISO data are available at https://doi.org/10.48670/moi-00021 and https://doi.org/10.48670/mds-00327. CESM LENS-2 data are available at https://esd.copernicus.org/articles/12/1393/2021/esd-12-1393-2021.html. SMAP salinity data are available at https://podaac.jpl.nasa.gov/dataset/SMAP_RSS_L3_SSS_SMI_MONTHLY_V6. High-frequency radar data are available at https://dods.ndbc.noaa.gov/thredds/catalog/hfradar.html?dataset=hfradar_uswc_6km_25hravg. Sentinel-3 OLCI data are available at https://doi.org/10.48670/moi-00278, and MODIS Aqua data are available at https://doi.org/10.5067/AQUA/MODIS/L3M/CHL/2022.0.

Conflict of Interest declaration

The authors declare there are no conflicts of interest for this manuscript.

Acknowledgments

The authors are grateful to Pat Kelly, Dawn Outram, the S-MODE science team, the captain and crew of the R/V Sally Ride, and NASA grants 80NSSC24M0143 and 80NSSC24K1422.

Author contributions: S. Gangrade: Conceptualization, Data curation, Formal analysis, Investigation, Methodology, Visualization, Writing - original draft, Writing - review & editing; **M. A. Freilich**: Conceptualization, Data curation, Formal analysis, Investigation, Methodology, Visualization, Writing - original draft, Writing - review & editing; **É. Beaudin**: Formal analysis, Investigation, Methodology, Visualization, Writing - review & editing; **K. Luis**: Investigation, Methodology, Writing - review & editing; **I. M. Leyba**: Formal analysis, Writing - review & editing, **M. M. Omand**: Investigation, Writing - review & editing; **S. E. Lang**: Investigation, Writing - review & editing; **J. Bowman**: Investigation, Methodology, Writing - review & editing.; **L. O'Neill**: Investigation, Writing - review & editing; ; **D. Capone**: Investigation, Writing - review & editing.

References

Barbera, P., Kozlov, A. M., Czech, L., Morel, B., Darriba, D., Flouri, T., & Stamatakis, A. (2019, March). EPA-ng: Massively Parallel Evolutionary Placement of Genetic Sequences. *Systematic Biology*, *68*(2), 365–369. Retrieved 2026-03-10, from https://academic.oup.com/sysbio/article/68/2/365/5079844 doi: 10.1093/sysbio/syy054

Bartusek, S. T., Seo, H., Ummenhofer, C. C., & Steffen, J. (2021). The Role of Nearshore Air-Sea Interactions for Landfalling Atmospheric Rivers on the U.S. West Coast. *Geophysical Research Letters*, *48*(6), e2020GL091388. Retrieved 2024-07-05, from https://onlinelibrary.wiley.com/doi/abs/10.1029/2020GL091388 doi: 10.1029/2020GL091388

Bowman, J. S., & Ducklow, H. W. (2015, August). Microbial Communities Can Be Described by Metabolic Structure: A General Framework and Application to a Seasonally Variable, Depth-Stratified Microbial Community from the Coastal West Antarctic Peninsula. *PLOS ONE*, *10*(8), e0135868. Retrieved 2026-01-07, from https://dx.plos.org/10.1371/journal.pone.0135868 doi: 10.1371/journal.pone.0135868

Callahan, B. J., McMurdie, P. J., Rosen, M. J., Han, A. W., Johnson, A. J. A., & Holmes, S. P. (2016, July). DADA2: High-resolution sample inference from Illumina amplicon data. *Nature Methods*, *13*(7), 581–583. Retrieved 2026-03-10, from https://www.nature.com/articles/nmeth.3869 doi: 10.1038/nmeth.3869

Catlett, D., Siegel, D., Simons, R., Guillocheau, N., Henderikx-Freitas, F., &

Thomas, C. (2021, September). Diagnosing seasonal to multi-decadal phytoplankton group dynamics in a highly productive coastal ecosystem. *Progress in Oceanography*, *197*, 102637. Retrieved 2026-01-07, from https://linkinghub.elsevier.com/retrieve/pii/S0079661121001221 doi: 10.1016/j.pocean.2021.102637

Cloern, J. E., Schraga, T. S., Nejad, E., & Martin, C. (2020, September). Nutrient Status of San Francisco Bay and Its Management Implications. *Estuaries and Coasts*, *43*(6), 1299–1317. Retrieved 2025-07-10, from https://doi.org/10.1007/s12237-020-00737-w doi: 10.1007/s12237-020-00737-w

Czech, L., Barbera, P., & Stamatakis, A. (2020, May). Genesis and Gappa: processing, analyzing and visualizing phylogenetic (placement) data. *Bioinformatics*, *36*(10), 3263–3265. Retrieved 2026-03-10, from https://academic.oup.com/bioinformatics/article/36/10/3263/5722201 doi: 10.1093/bioinformatics/btaa070

DeFlorio, M. J., Sengupta, A., Castellano, C. M., Wang, J., Zhang, Z., Gershunov, A., ... Anderson, M. L. (2024, January). From California's Extreme Drought to Major Flooding: Evaluating and Synthesizing Experimental Seasonal and Subseasonal Forecasts of Landfalling Atmospheric Rivers and Extreme Precipitation during Winter 2022/23. *Bulletin of the American Meteorological Society*, *105*(1), E84–E104. Retrieved 2026-03-02, from https://journals.ametsoc.org/view/journals/bams/105/1/BAMS-D-22-0208.1.xml doi: 10.1175/BAMS-D-22-0208.1

Durkin, C. A., Van Mooy, B. A. S., Dyhrman, S. T., & Buesseler, K. O. (2016, July). Sinking phytoplankton associated with carbon flux in the Atlantic Ocean. *Limnology and Oceanography*, *61*(4), 1172–1187. Retrieved 2026-01-13, from https://aslopubs.onlinelibrary.wiley.com/doi/10.1002/lno.10253 doi: 10.1002/lno.10253

Farrar, J. T., D'Asaro, E., Rodríguez, E., Shcherbina, A., Lenain, L., Omand, M., ... Westbrook, E. (2025, April). S-MODE: The Sub-Mesoscale Ocean Dynamics Experiment. *Bulletin of the American Meteorological Society*, *106*(4), E657–E677. Retrieved 2026-01-07, from https://journals.ametsoc.org/view/journals/bams/106/4/BAMS-D-23-0178.1.xml doi: 10.1175/BAMS-D-23-0178.1

Gangrade, S., Franks, P. J. S., Forsch, K. O., & Barbeau, K. A. (2025, December). Salinity is diagnostic of maximum potential chlorophyll and phytoplankton community structure in an Eastern Boundary Upwelling System. *Limnology and Oceanography Letters*, *10*(6), 923–933. Retrieved 2026-01-07, from https://aslopubs.onlinelibrary.wiley.com/doi/10.1002/lol2.70059 doi: 10.1002/lol2.70059

Gershunov, A., Shulgina, T., Clemesha, R. E. S., Guirguis, K., Pierce, D. W., Dettinger, M. D., ... Ralph, F. M. (2019, July). Precipitation regime change in Western North America: The role of Atmospheric Rivers. *Scientific Reports*, *9*(1), 9944. Retrieved 2026-03-02, from https://www.nature.com/articles/s41598-019-46169-w doi: 10.1038/s41598-019-46169-w

Gruber, N., Lachkar, Z., Frenzel, H., Marchesiello, P., Münnich, M., McWilliams, J. C., ... Plattner, G.-K. (2011). Eddy-induced reduction of biological production in eastern boundary upwelling systems. *Nature Geoscience*, *4*(11), 787–792.

Guillou, L., Bachar, D., Audic, S., Bass, D., Berney, C., Bittner, L., ... Christen, R. (2012, November). The Protist Ribosomal Reference database (PR2): a catalog of unicellular eukaryote Small Sub-Unit rRNA sequences with curated taxonomy. *Nucleic Acids Research*, *41*(D1), D597–D604. Retrieved 2026-03-10, from http://academic.oup.com/nar/article/41/D1/D597/1064851/The-Protist-Ribosomal-Reference-database-PR2-a doi: 10.1093/nar/gks1160

Higgins, T. B., Subramanian, A. C., Watson, P. A. G., & Sparrow, S. (2025, March). Changes to Atmospheric River Related Extremes Over the United States West Coast Under Anthropogenic Warming. *Geophysical Research Letters*, *52*(5), e2024GL112237. Retrieved 2026-03-02, from https://agupubs.onlinelibrary.wiley.com/doi/10.1029/2024GL112237 doi: 10.1029/2024GL112237

Hoffman, L., Mazloff, M. R., Gille, S. T., Giglio, D., & Varadarajan, A. (2022, August). Ocean Surface Salinity Response to Atmospheric River Precipitation in the California Current System. *Journal of Physical Oceanography*, *52*(8), 1867–1885. Retrieved 2023-12-06, from https://journals.ametsoc.org/view/journals/phoc/52/8/JPO-D-21-0272.1.xml doi: 10.1175/JPO-D-21-0272.1

Hogle, S. L., Dupont, C. L., Hopkinson, B. M., King, A. L., Buck, K. N., Roe, K. L., ... Barbeau, K. A. (2018, December). Pervasive iron limitation at subsurface chlorophyll maxima of the California Current. *Proceedings of the National Academy of Sciences*, *115*(52), 13300–13305. Retrieved 2025-07-06, from https://www.pnas.org/doi/abs/10.1073/pnas.1813192115 doi: 10.1073/pnas.1813192115

Jacox, M. G., Edwards, C. A., Hazen, E. L., & Bograd, S. J. (2018, October). Coastal Upwelling Revisited: Ekman, Bakun, and Improved Upwelling Indices for the U.S. West Coast. *Journal of Geophysical Research: Oceans*, *123*(10), 7332–7350. Retrieved 2026-01-07, from https://agupubs.onlinelibrary.wiley.com/doi/10.1029/2018JC014187 doi: 10.1029/2018JC014187

Jhugroo, K., O'Callaghan, J. M., & Stevens, C. L. (2024, July). The impact of high rainfall events on the submesoscale salinity field in a coastal sea: Greater Cook Strait, New Zealand. *New Zealand Journal of Marine and Freshwater Research*, 1–27. Retrieved 2024-08-02, from https://www.tandfonline.com/doi/full/10.1080/00288330.2024.2368853 doi: 10.1080/00288330.2024.2368853

Jimenez Arellano, C., Rouzegari, N., Dao, V., Bolboli Zadeh, M., Shearer, E., Afzali Gorooh, V., ... Sorooshian, S. (2025, May). Beyond Expectations: Investigating Anomalous 2022–23 Winter Weather Conditions and Water Resources Impacts in California. *Bulletin of the American Meteorological Society*, *106*(5), E920–E938. Retrieved 2026-03-02, from https://journals.ametsoc.org/view/journals/bams/106/5/BAMS-D-23-0336.1.xml doi: 10.1175/BAMS-D-23-0336.1

Johnson, K. S., Chavez, F. P., & Friederich, G. E. (1999, April). Continental-shelf sediment as a primary source of iron for coastal phytoplankton. *Nature*, *398*(6729), 697–700. Retrieved 2025-07-06, from https://www.nature.com/articles/19511 doi: 10.1038/19511

Kessouri, F., McWilliams, J. C., Bianchi, D., Sutula, M., Renault, L., Deutsch, C., ... Weisberg, S. B. (2021, May). Coastal eutrophication drives acidification, oxygen loss, and ecosystem change in a major oceanic upwelling system. *Proceedings of the National Academy of Sciences*, *118*(21). Retrieved 2021-05-27, from https://www.pnas.org/content/118/21/e2018856118 doi: 10.1073/pnas.2018856118

Kramer, S. J., Jones, E. L., Estapa, M. L., Paul, N. L., Rynearson, T. A., Santoro, A. E., ... Durkin, C. A. (2025, January). Sinking particles exporting diatoms and Hacrobia predict the magnitude of oceanic POC flux. *The ISME Journal*, *19*(1), wraf105. Retrieved 2026-01-13, from https://academic.oup.com/ismej/article/doi/10.1093/ismejo/wraf105/8140949 doi: 10.1093/ismejo/wraf105

Kudela, R. M., & Chavez, F. P. (2004, May). The impact of coastal runoff on ocean color during an El Niño year in Central California. *Deep Sea Research Part II: Topical Studies in Oceanography*, *51*(10), 1173–1185. Retrieved

2025-07-06, from https://www.sciencedirect.com/science/article/pii/S0967064504001067 doi: 10.1016/j.dsr2.2004.04.002

Lagos-Zúñiga, M., Mendoza, P. A., Campos, D., & Rondanelli, R. (2024, January). Trends in seasonal precipitation extremes and associated temperatures along continental Chile. *Climate Dynamics*. Retrieved 2024-02-08, from https://doi.org/10.1007/s00382-024-07127-z doi: 10.1007/s00382-024-07127-z

Lang, S. E., Omand, M., & Kelly, R. P. (2023). *S-MODE Shipboard Bio-optical Measurements Version 1.* NASA Physical Oceanography Distributed Active Archive Center. Retrieved 2026-03-02, from https://earthdata.nasa.gov/data/catalog/pocloud-smode-l2-shipboard-bio-v1-1 doi: 10.5067/SMODE-RVBO2

Legendre, P., & Gallagher, E. D. (2001, October). Ecologically meaningful transformations for ordination of species data. *Oecologia*, *129*(2), 271–280. Retrieved 2026-01-12, from http://link.springer.com/10.1007/s004420100716 doi: 10.1007/s004420100716

Marchetti, A., Schruth, D. M., Durkin, C. A., Parker, M. S., Kodner, R. B., Berthiaume, C. T., ... Armbrust, E. V. (2012, February). Comparative metatranscriptomics identifies molecular bases for the physiological responses of phytoplankton to varying iron availability. *Proceedings of the National Academy of Sciences*, *109*(6). Retrieved 2026-01-15, from https://pnas.org/doi/full/10.1073/pnas.1118408109 doi: 10.1073/pnas.1118408109

McWilliams, J. C., Gula, J., Molemaker, M. J., Renault, L., & Shchepetkin, A. F. (2015). Filament frontogenesis by boundary layer turbulence. *Journal of Physical Oceanography*, *45*(8), 1988–2005.

Merz, E., Hale, R. J., Saberski, E., Kenitz, K. M., Carter, M. L., Bowman, J. S., & Barton, A. D. (2026, January). Temperature alters interactions and keystone taxa in the marine microbiome. *The ISME Journal*, *20*(1), wraf287. Retrieved 2026-03-10, from https://academic.oup.com/ismej/article/doi/10.1093/ismejo/wraf287/8407146 doi: 10.1093/ismejo/wraf287

Nagai, T., Gruber, N., Frenzel, H., Lachkar, Z., McWilliams, J. C., & Plattner, G.-K. (2015). Dominant role of eddies and filaments in the offshore transport of carbon and nutrients in the California Current System. *Journal of Geophysical Research: Oceans*, *120*(8), 5318–5341. Retrieved 2024-12-20, from https://onlinelibrary.wiley.com/doi/abs/10.1002/2015JC010889 doi: 10.1002/2015JC010889

Nawrocki, E. P., & Eddy, S. R. (2013, November). Infernal 1.1: 100-fold faster RNA homology searches. *Bioinformatics*, *29*(22), 2933–2935. Retrieved 2026-03-10, from https://academic.oup.com/bioinformatics/article/29/22/2933/316439 doi: 10.1093/bioinformatics/btt509

Oksanen, J., Simpson, G. L., Blanchet, F. G., Kindt, R., Legendre, P., Minchin, P. R., ... Weedon, J. (2001, September). *vegan: Community Ecology Package.* Retrieved 2026-01-12, from https://CRAN.R-project.org/package=vegan (Institution: Comprehensive R Archive Network Pages: 2.7-2) doi: 10.32614/CRAN.package.vegan

O'Leary, N. A., Wright, M. W., Brister, J. R., Ciufo, S., Haddad, D., McVeigh, R., ... Pruitt, K. D. (2016, January). Reference sequence (RefSeq) database at NCBI: current status, taxonomic expansion, and functional annotation. *Nucleic Acids Research*, *44*(D1), D733–D745. Retrieved 2026-03-10, from https://academic.oup.com/nar/article-lookup/doi/10.1093/nar/gkv1189 doi: 10.1093/nar/gkv1189

Palacios, D. M., Hazen, E. L., Schroeder, I. D., & Bograd, S. J. (2013, July). Modeling the temperature-nitrate relationship in the coastal upwelling domain of the California Current: Modeling the T-N Relationship. *Journal of Geophysical Research: Oceans*, *118*(7), 3223–3239. Retrieved 2026-01-16, from http://doi.wiley.com/10.1002/jgrc.20216 doi: 10.1002/jgrc.20216

Ralph, F. M., Neiman, P. J., Wick, G. A., Gutman, S. I., Dettinger, M. D., Cayan, D. R., & White, A. B. (2006). Flooding on California's Russian River: Role of atmospheric rivers. *Geophysical Research Letters*, *33*(13). Retrieved 2023-12-06, from https://onlinelibrary.wiley.com/doi/abs/10.1029/2006GL026689 doi: 10.1029/2006GL026689

Regnier, P., Resplandy, L., Najjar, R. G., & Ciais, P. (2022, March). The land-to-ocean loops of the global carbon cycle. *Nature*, *603*(7901), 401–410. Retrieved 2024-02-08, from https://www.nature.com/articles/s41586-021-04339-9 doi: 10.1038/s41586-021-04339-9

Rodríguez, E., Wineteer, A., Perkovic-Martin, D., Gál, T., Stiles, B. W., Niamsuwan, N., & Rodriguez Monje, R. (2018, April). Estimating Ocean Vector Winds and Currents Using a Ka-Band Pencil-Beam Doppler Scatterometer. *Remote Sensing*, *10*(4), 576. Retrieved 2026-02-04, from https://www.mdpi.com/2072-4292/10/4/576 doi: 10.3390/rs10040576

Roesler, C. S., & Barnard, A. H. (2013, September). Optical proxy for phytoplankton biomass in the absence of photophysiology: Rethinking the absorption line height. *Methods in Oceanography*, *7*, 79–94. Retrieved 2026-03-02, from https://linkinghub.elsevier.com/retrieve/pii/S2211122013000509 doi: 10.1016/j.mio.2013.12.003

Seitz, L. R., & Freilich, M. A. (2025, April). Joint Effects of Submesoscale Lateral Dispersion and Biological Reactions on Biogeochemical Flux. *Geophysical Research Letters*, *52*(7), e2024GL114112. Retrieved 2026-01-07, from https://agupubs.onlinelibrary.wiley.com/doi/10.1029/2024GL114112 doi: 10.1029/2024GL114112

Swain, D. L., Langenbrunner, B., Neelin, J. D., & Hall, A. (2018, May). Increasing precipitation volatility in twenty-first-century California. *Nature Climate Change*, *8*(5), 427–433. Retrieved 2023-08-08, from https://www.nature.com/articles/s41558-018-0140-y doi: 10.1038/s41558-018-0140-y

Taylor, A. G., Landry, M. R., Selph, K. E., & Wokuluk, J. J. (2015, February). Temporal and spatial patterns of microbial community biomass and composition in the Southern California Current Ecosystem. *Deep Sea Research Part II: Topical Studies in Oceanography*, *112*, 117–128. Retrieved 2026-01-16, from https://linkinghub.elsevier.com/retrieve/pii/S0967064514000502 doi: 10.1016/j.dsr2.2014.02.006

Teeling, H., Fuchs, B. M., Becher, D., Klockow, C., Gardebrecht, A., Bennke, C. M., ... Amann, R. (2012, May). Substrate-Controlled Succession of Marine Bacterioplankton Populations Induced by a Phytoplankton Bloom. *Science*, *336*(6081), 608–611. Retrieved 2026-01-07, from https://www.science.org/doi/10.1126/science.1218344 doi: 10.1126/science.1218344

Teeling, H., Fuchs, B. M., Bennke, C. M., Krüger, K., Chafee, M., Kappelmann, L., ... Amann, R. I. (2016, April). Recurring patterns in bacterioplankton dynamics during coastal spring algae blooms. *eLife*, *5*, e11888. Retrieved 2026-01-07, from https://elifesciences.org/articles/11888 doi: 10.7554/eLife.11888

Wineteer, A., Perkovic-Martin, D., Monje, R., Rodríguez, E., Gál, T., Niamsuwan, N., ... Stiles, B. (2020, March). Measuring Winds and Currents with Ka-Band Doppler Scatterometry: An Airborne Implementation and Progress towards a Spaceborne Mission. *Remote Sensing*, *12*(6), 1021. Retrieved 2026-02-04, from https://www.mdpi.com/2072-4292/12/6/1021 doi: 10.3390/rs12061021

Zaba, K. D., Franks, P. J. S., & Ohman, M. D. (2021). The California Undercurrent as a Source of Upwelled Waters in a Coastal Filament. *Journal of Geophysical Research: Oceans*, *126*(2), e2020JC016602. Retrieved 2021-02-26, from https://agupubs.onlinelibrary.wiley.com/doi/abs/10.1029/2020JC016602 doi: https://doi.org/10.1029/2020JC016602